ELSEVIER

Sensors and Actuators 78 (1999) 74–80

SENSORS AND ACTUATORS A PHYSICAL

www.elsevier.nl/locate/sna

Low creep and hysteresis load cell based on a force-to-fluid pressure transformation

Robert A.F. Zwijze *, Remco J. Wiegerink, Gijs J.M. Krijnen, Theo S.J. Lammerink, Miko Elwenspoek

Mesa Research Institute, University of Twente, P.O. Box 217, 7500 AE Enschede, Netherlands

Received 13 August 1998; received in revised form 17 February 1999; accepted 22 February 1999

Abstract

In this paper, a low-cost load cell (force sensor) is presented in which the force to be measured is transformed into a fluid pressure. The design consists of a boss, attached to a membrane, and a bucket-like structure which encloses a fluid volume. This geometry causes a force to be transformed into a pressure. We show that this transformation only depends on the geometrical parameters of the load cell and that it is independent of the Young's modulus of the membrane resulting in very low creep and hysteresis. Experimental results with loads up to 1000 kg show very good repeatability and are in close agreement with both analytical and numerical calculations. © 1999 Elsevier Science S.A. All rights reserved.

Keywords: Load cell; Force measurement

1. Introduction

Load cells are used in, for example, weighing bridges for lorries, cars and trailers. Also in bulk industries, it is necessary to measure weights as accurately as possible. Most current load cells are made of steel. The performance of these load cells is limited by hysteresis and creep even when expensive high-grade steels are used.

The load cell we are aiming at has the following specifications.

- maximum load: 10 000 N (1000 kg)
- full scale accuracy: 0.03% = 0.3 kg
- temperature range: −10 to 50°C
- production costs: less than US$75
- calibration: once in 2 years

The load cell discussed in this paper is shown in Fig. 1. It consists of a bucket in which a fluid is sealed by a membrane. A Viton™ seal is used to prevent leakage. The force is applied to a boss which is attached to the center of the membrane. Due to this (positive) force, the boss is displaced downwards and the fluid is pressed away from beneath the boss. As the fluid cannot escape, the pressure increases. This pressure and the shear force in the membrane carry the force which is applied to the boss. It will be shown that the pressure difference between the fluid and the air is independent of the Young's modulus of the membrane which means that the pressure is independent of creep and hysteresis in the membrane.

In Ref. [1], a force-to-fluid pressure transformation was introduced for application in a new kind of load cell. This load cell consists of a piston under which the fluid is seated. Characteristic for this load cell is its high sensitivity. However, its sensitivity to hysteresis is probably large, because the pressure–force relation is a function of the Young's modulus of the screws which are used. Another disadvantage is that it needs a Teflon seal and a proper surface finish of the mating steel parts to enclose the fluid. The load cell discussed in this paper does not have these drawbacks. It only needs a Viton™ ring for sealing the fluid. As a membrane is used to enclose the fluid, a proper surface finish of the mating steel part is not necessary. In Section 2, a model of the load cell is presented. In Section 2.1, the pressure–force relation is derived under the assumption of incompressibility of the fluid. In Section 2.2, the compressibility is incorporated into the calculations. In Section 2.3, the stresses in the membrane are calculated under the assumption of incompressibility of the fluid. The pressure dependence on temperature is analyzed in Sec-

* Corresponding author. Tel.: +31-53-4894-373; fax: +31-53-4893-343; e-mail: a.f.zwijze@el.utwente.nl

PII: S0924-4247(99)00079-5

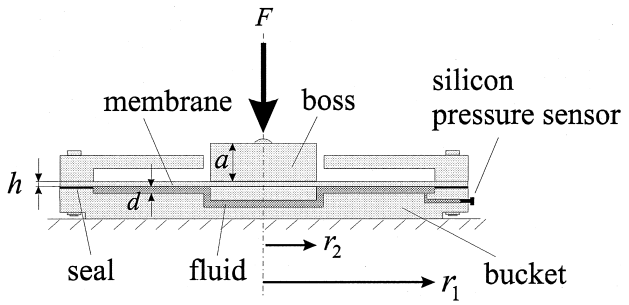

Fig. 1. Layout of the force-to-fluid pressure load cell. The force presses the boss downward. This causes a pressure increase in the fluid. The membrane encloses the fluid in the bucket.

tions 2.4 and 2.5. Finite element calculations are presented in Section 2.6. The realized prototype and experimental results are presented in Section 3. Finally, conclusions are drawn in Section 4.

2. Modeling

In this section, the load cell is modeled and analyzed analytically and numerically.

2.1. Pressure–force relation for incompressible fluid

In Fig. 2, a schematic drawing of the deformation profile of the membrane and the deflection of the boss for some load F is shown. T is the shear force between the membrane and the boss. The pressure difference P_s between the fluid and the air acts on the membrane and the boss. Equilibrium of forces for the boss is given by

$$T = F - P_s \pi r_2^2. \tag{1}$$

The deflection profile $w(r)$ of the membrane has to satisfy the following boundary conditions.

$$w(r_1) = 0, \quad \frac{\mathrm{d}w}{\mathrm{d}r}(r_1) = \frac{\mathrm{d}w}{\mathrm{d}r}(r_2) = 0 \tag{2}$$

Using elasticity theory for plates [2], it can be derived from Eqs. (1) and (2) that

$$w(r) = \frac{F(1-\upsilon^2)}{Eh^3} g_1(r, r_1, r_2) + \frac{P_s(1-\upsilon^2)}{Eh^3} g_2(r, r_1, r_2), \tag{3}$$

where g_1 and g_2 are functions of r, r_1 and r_2. υ is the Poisson's ratio and E the Young's modulus of the membrane. By assuming incompressibility of the fluid, the volume is constant under deformation of the membrane:

$$\pi r_2^2 w(r_2) + \int_{r=r_2}^{r_1} 2\pi r w(r)\,\mathrm{d}r = 0. \tag{4}$$

The pressure–force relation is derived from Eqs. (3) and (4), yielding

$$P_s = \frac{F}{A_{\text{eff}}},$$

$$A_{\text{eff}} = \frac{\pi r_2^2}{\pi} \times \frac{(1 - 4s^2 + 6s^4 - 4s^6 + s^8)}{(3.82\ln(s)[s^2 - s^4] + 0.95[1 - s^2 - s^4 + s^6])},$$

$$s = \frac{r_1}{r_2}. \tag{5}$$

A_{eff} is called the effective area. Eq. (5) shows that the pressure–force relation only depends on the geometrical dimensions and not on the Young's modulus of the membrane. The change of these parameters is a only a second-order effect which is not shown by (first-order) linear elasticity theory. Therefore, it can be expected that the force-to-fluid pressure transformation has low sensitivity to creep and hysteresis in the membrane. An impression of the effective area in comparison to the total area of the bucket (= area boss + area membrane) and the area of the boss is shown in Fig. 3. From this figure, it can be concluded that the effective area lies somewhere between the area of the boss and the area of the bucket, because $\pi r_2^2 < A_{\text{eff}} < \pi r_1^2$. For a ratio r_1/r_2 approaching one, the effective area approaches πr_2^2 so that from Eqs. (1) and (5), it follows that the shear force T in the membrane becomes zero. For the parameters given in the caption of Fig. 4, the pressure–force sensitivity is calculated from Eq. (5) giving $\partial P_s/\partial F = 47.9086$ Pa/N. The values of the geometric parameters will be explained in Section 2.2 to Section 2.5.

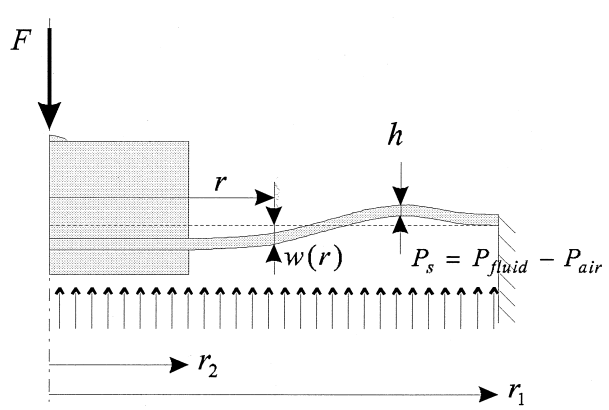

Fig. 2. Deformation of the membrane. $w(r)$ represents the deflection of the membrane at position r.

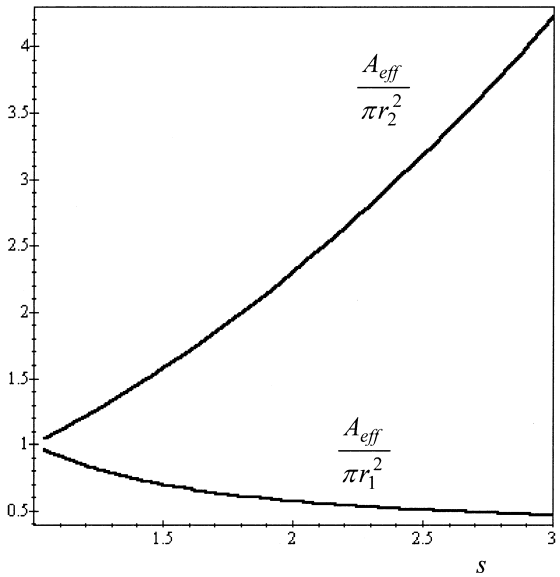

Fig. 3. Effective area divided by the area of the bucket and effective area divided by the area of the boss as a function of the ratio $s = r_1 / r_2$.

The expression for the deflection $w(r)$ of the membrane follows from Eqs. (3) and (5) giving

$$w(r) = \frac{F(\upsilon^2 - 1)}{Eh^3}\lambda\left(s = \frac{r_1}{r_2}, r_1, r\right), \tag{6}$$

where $\lambda(r_1/r_2, r_1, r)$ is a rather complex function. An impression of the deformation of the membrane for some chosen parameters is shown in Fig. 4 where the membrane is assumed to be made of steel.

2.2. Pressure–force relation for compressible fluid

By including compressibility of the fluid [3], Eq. (4) becomes

$$\pi r_2^2 w(r_2) + \int_{r=r_2}^{r_1} 2\pi r w(r)\,\mathrm{d}r = \Delta V = V_0 \frac{P_s}{E_\upsilon}, \tag{7}$$

where E_υ is the bulk compressibility modulus, V_0 the initial volume and ΔV the decrease in volume of the compressed fluid. For water, $E_\upsilon = 2.24$ GN/m^2. The effective area is calculated the same way as before, giving

$$A_{\text{eff}} = \pi r_2^2 \frac{\left\{1 - 3s^2 + 3s^4 - s^6 + \dfrac{16V_0 Eh^3}{\pi E_\upsilon r_1^6(\upsilon^2 - 1)} s^6\right\}}{3.82\ln(s)\, s^2 + 0.95[1 - s^4]}. \tag{8}$$

We see that the Young's modulus appears in this equation, therefore the term $\dfrac{16V_0 Eh^3}{\pi E_\upsilon r_1^6(\upsilon^2 - 1)}$ must be made as small as possible. The simplest method to reduce this term is by taking a very small initial fluid volume. For the parameters in the caption of Fig. 4, the pressure sensitivity now equals $\partial P_s/\partial F = 47.9082$ Pa/N which only deviates 0.0008% from the incompressible case. So it is concluded that the assumption of incompressibility can be maintained. From now on, it will be assumed in the analytical calculations that the fluid is incompressible.

2.3. Mechanical stresses in the membrane

As the membrane is rather thin, it must be checked whether the yield stress is not exceeded, because this would lead to plastic deformation of the membrane.

In the membrane, three stresses are present: radial, tangential and shear stress which is acting in the direction of force F (σ_r, σ_t and τ, respectively). The first two are calculated from their corresponding moments [2] and they have a maximum on the top and bottom sides of the membrane. As all three stresses occur at the same place in the membrane, the Von Mises stress criterion is used to determine the maximum allowable stress. It is given by [4]

$$\sigma_V = \sqrt{\frac{1}{2}\left[(\sigma_r - \sigma_t)^2 + \sigma_t^2 + \sigma_r^2 + 6\tau^2\right]}. \tag{9}$$

A plot of all the stresses is shown in Fig. 5 (the parameters shown in Fig. 4 are used). The yield stress of steel is about 1.5 Gpa [5], so it should be possible to bear a load of 10 000 N.

A simple expression for σ_υ can be obtained by neglecting the shear stress τ. It can be shown that this stress is very small in comparison to σ_r and σ_t. For a ratio $s = r_1/r_2$ approaching one, at the boss, τ even becomes zero, because (as was already concluded) the shear force T becomes zero. It is seen that the maximum stresses occur

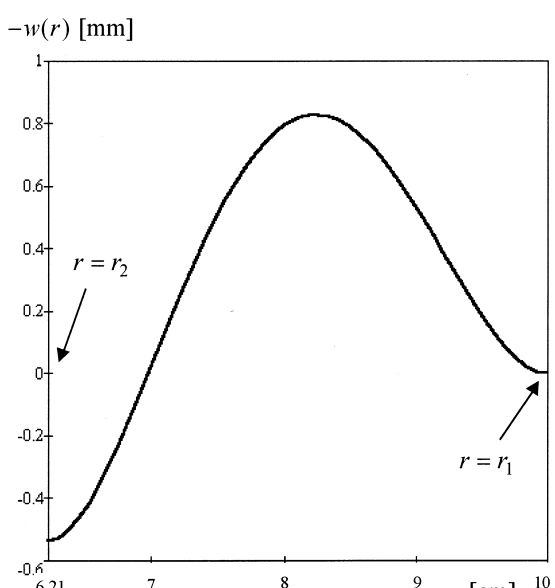

Fig. 4. Deformation of the steel membrane ($F = 10\,000$ N, $E = 210$ GPa, $\upsilon = 0.3$, $h = 0.5$ mm, $r_1 = 10$ cm, $r_2 = 6.21$ cm, $d = 1$ mm and $a = 2.5$ cm).

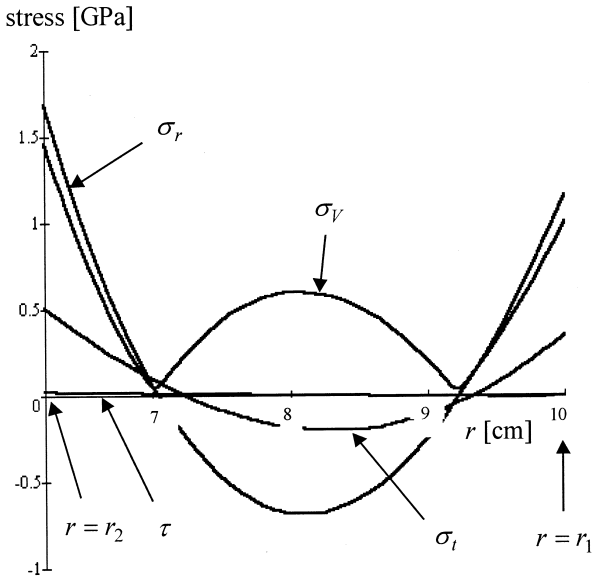

Fig. 5. Radial, tangential, shear and Von Mises stresses in the membrane.

at $r = r_2$. Therefore, the maximum Von Mises stress in the membrane is approximately given by

$$\sigma_{V,\max} = \frac{3F\sqrt{(1-\upsilon-\upsilon^2)}}{4\pi h^2}\gamma(s),$$

$$\gamma(s) = \frac{(4\ln(s)s^4 - 5s^4 + 8\ln(s)s^2 + 4s^2 + 1)}{(1-2s^2+s^4)}. \quad (10)$$

The function $\gamma(s)$ is drawn in Fig. 6. It is concluded that the maximum stress can be reduced for a large membrane thickness and a ratio $s = r_1/r_2$ approaching one.

2.4. Dependence of effective area on temperature

For describing the effective area as a function of the temperature change T, r_1 and r_2 must be written as a function of temperature. For a thermal expansion coefficient $\alpha_{\text{boss/membrane}}$ of the boss and membrane, they are given by

$$r_1 = r_{1,0}(1 + \alpha_{\text{boss/membrane}}T)$$

and

$$r_2 = r_{2,0}(1 + \alpha_{\text{boss/membrane}}T), \quad (11)$$

where $r_{1,0}$ and $r_{2,0}$ are the radii for $T = 0$. Then, from Eqs. (5) and (11), it follows that for small temperature changes,

$$\frac{\frac{\mathrm{d}A_{\text{eff}}}{\mathrm{d}T}}{A_{\text{eff}}} = 2\alpha_{\text{boss/membrane}}. \quad (12)$$

The resulting maximum error for a maximum temperature increase $T_{\max}$ is given by

$$\varepsilon_{A_{\text{eff}}} = 2\alpha_{\text{boss/membrane}}T_{\max}. \quad (13)$$

For a steel boss and membrane $\alpha_{\text{boss/membrane}} = 12\times10^{-6}$ °C^{-1} so that for a maximum temperature increase $T_{\max} =$ 30°C, the error is only 0.07%. This error can be compensated for by measuring the temperature.

2.5. Dependence of pressure on temperature due to difference in thermal expansion coefficients of bucket and fluid

Another temperature effect is caused by the difference in thermal expansion coefficients of the bucket and fluid. In order to model this effect, Eq. (4) is changed to

$$\pi r_2^2 w(r=r_2) + \int_{r=r_2}^{r_1} 2\pi r w(r)\mathrm{d}r = -V_0 3(\alpha_{\text{fluid}} - \alpha_{\text{bucket}})T. \quad (14)$$

By setting F equal to zero, it follows from Eqs. (3) and (14) that the pressure–temperature sensitivity is given by

$$\frac{\mathrm{d}P_s}{\mathrm{d}T} = 15.29\frac{s^6h^3E(\alpha_{\text{fluid}} - \alpha_{\text{bucket}})V_0}{(1-\upsilon^2)r_1^6(s^6 - 3s^4 + 3s^2 - 1)}. \quad (15)$$

The pressure variation (error) which is introduced by temperature variations is considered with respect to the pressure at full load ($F_{\max} = 10\,000$ N). Therefore, in minimizing the temperature error, one has to minimize

$$\varepsilon_{\Delta\alpha} = \frac{\left(\frac{\mathrm{d}P_s}{\mathrm{d}T}T_{\max}\right)}{\left(\frac{\mathrm{d}P_s}{\mathrm{d}F}F_{\max}\right)}. \quad (16)$$

Substitution of Eqs. (5) and (15) in Eq. (16) gives

$$\varepsilon_{\Delta\alpha} = \frac{16T_{\max}V_0(\alpha_{\text{fluid}} - \alpha_{\text{bucket}})Eh^3}{F_{\max}r_1^4}\kappa(s,\upsilon),$$

$$\kappa(s,\upsilon) = \frac{s^4}{((1-\upsilon^2)s^4 - (1-\upsilon^2)\ln(s)s^2 - 1 + \upsilon^2)}. \quad (17)$$

So, it can be concluded that the fluid volume and Young's modulus should be minimized and that both thermal ex-

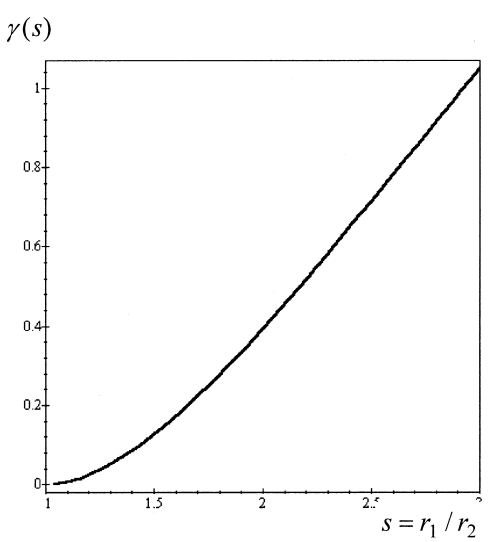

Fig. 6. Von Mises stress parameter $\gamma(s)$.

pansion coefficients must match as close as possible. It could also be concluded that h must be decreased, r_1 increased and s increased. However, one has to take into account that the change of these parameters leads to a change in the maximum Von Mises stress (see Eq. (10)). So, one has to incorporate the maximum Von Mises stress in Eq. (17), which is done by solving h from Eq. (10), resulting in

$$\varepsilon_{\Delta\alpha} = \frac{\Delta T_{\max}\sqrt{F_{\max}}\, V_0(\alpha_{\text{fluid}} - \alpha_{\text{bucket}})\, E}{\sigma_{V,\max}^{1.5}\, r_1^4}\beta(s,\upsilon^2). \qquad (18)$$

The function $\beta(s,\upsilon^2 = 0.3^2)$ is plotted in Fig. 7. It is concluded that the ratio $s = r_1/r_2$ should be chosen close to one and r_1 as large as possible. For water at 20°C, $\alpha_{\text{water}} = 207 \times 10^{-6}$ °C^{-1}. Then, for $T_{\max} = 30$°C, the error equals 0.07%. In this calculation, the parameters shown in Fig. 4 are used and it is assumed that the bucket is made of steel. Again this (small) error can be compensated for by measuring the temperature.

2.6. Finite element calculations

In order to support the analytical calculations, the load cell is also analyzed in the finite element program Ansys 5.3. For the (compressible) fluid, FLUID79 elements are taken. The point force is applied in the center of the boss. The element mesh is shown in Fig. 8. The numerical calculated pressure–force sensitivity varies in all elements between 45.4 and 48.8 Pa/N (the analytical value for the compressible and incompressible case equals $\partial P_s/\partial F =$ 47.9 Pa/N). This is due to the small height of the fluid. The elements deform too much which causes the spread. But when $d = 1$ cm is taken, then for all elements, $\partial P_s/\partial F = 47.90 \pm 0.01$ Pa/N is obtained.

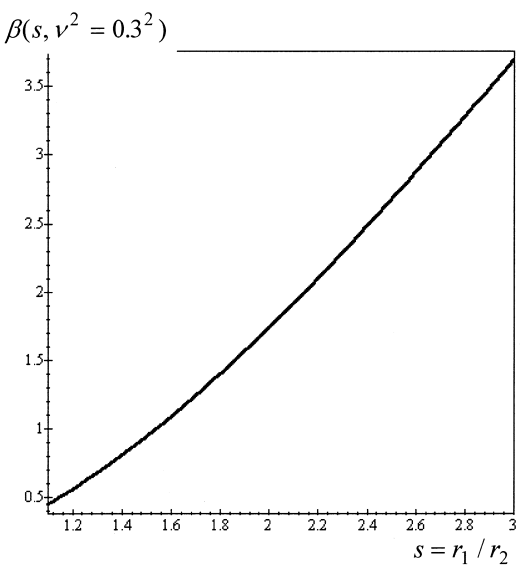

Fig. 7. Error parameter $\beta(s,\upsilon^2 = 0.3^2)$.

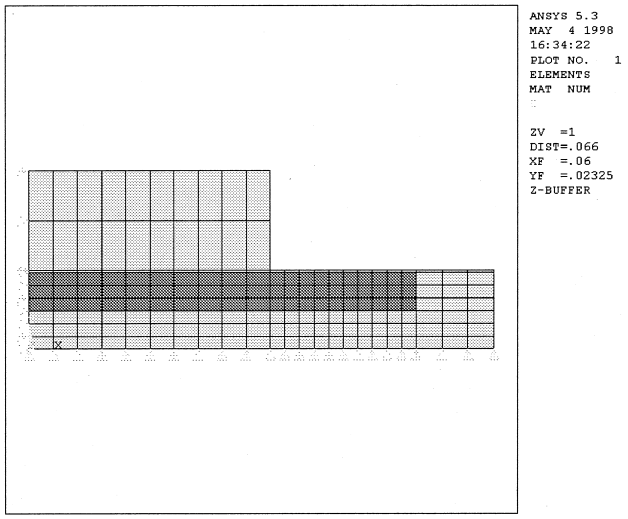

Fig. 8. Element mesh. For sake of clarity, the dimensions are not the same as in Fig. 4. In actual simulations, much more elements were used.

The temperature effect which was discussed in Section 2.4 cannot be checked in Ansys, because the numerical error is larger than this error. However, the temperature effect discussed in Section 2.5 can be analyzed in Ansys. This is done by taking $d = 1$ cm. Then Ansys calculates a pressure–temperature sensitivity of $\partial P_s/\partial T = 112.3 \pm 0.05$ Pa/°C. The analytical value follows from Eq. (15), giving $\partial P_s/\partial T = 116.6$ Pa/°C.

From the numerical calculations, it is concluded that the analytical formulas are correct and that they can be used to dimension the load cell.

3. Realization and experiments

In order to test the theory, a prototype has been realized in which the membrane and bucket are made of steel and are sealed with a rubber ring (Viton™). Bolts are used to

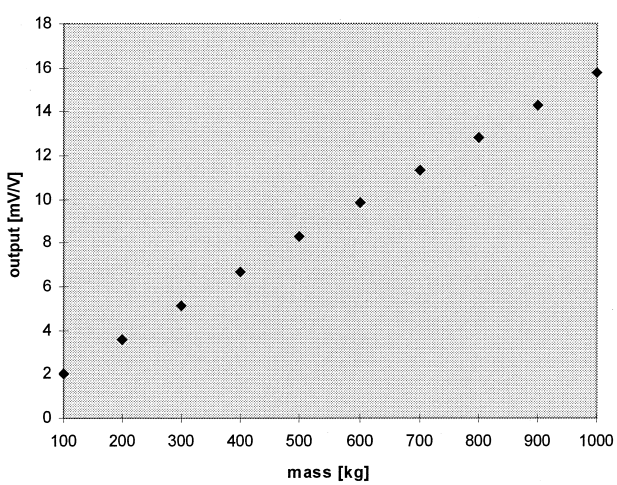

Fig. 9. Output Wheatstone bridge of the pressure sensor.

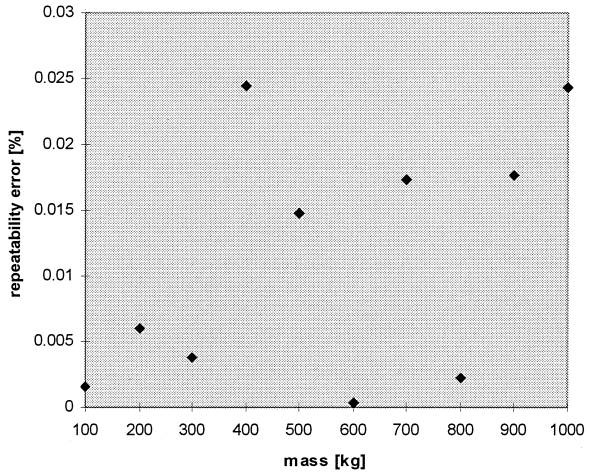

Fig. 10. Absolute value of the repeatability error in the output of the pressure sensor.

connect the different parts. The parameters are $E = 210$ GPa, $\upsilon = 0.3$, $h = 0.5$ mm, $r_1 = 10$ cm, $r_2 = 6.21$ cm, $d = 1$ mm and $a = 2.5$ cm (see also Fig. 4). The pressure was measured with a commercially available silicon pressure sensor, model Honeywell 24PCF. Repeatability and hysteresis of this sensor are within $\pm 0.15\%$ and its linearity within $\pm 1.0\%$ of full scale.

The load cell was tested by loading the load cell twice. Each loading was done for 60 s and each second, the pressure was measured. Weights were available in steps of 100 kg (± 2.5 kg) up to 1000 kg. As each measurement only took 120 s (including zero load measurement), temperature effects were eliminated. Longer measurements were not possible because of the temperature dependence of the pressure sensor. However, in practical situations, longer measuring times may be necessary. The average output (difference between loading and unloading) of the pressure sensor is shown in Fig. 9. The load cell behaves linearly and the experimental pressure sensitivity equals 48.1 Pa/N which is in close agreement with the analytical and numerical result (49.7 Pa/N). The repeatability error as a percentage of the output at maximum load is shown in Fig. 10. It is seen that this error is within 0.025%. This is a good result. It is not known how much of this error is caused by the pressure sensor. Measurements with a very accurate pressure sensor are necessary to reveal this.

4. Conclusions

The design and modeling of a force-to-fluid pressure load cell has been described. It is proven that the pressure–force relation is in first order only depending on the geometrical parameters of the load cell and is independent of the Young's modulus of the membrane under the assumption of an incompressible fluid.

By including compressibility of the fluid, the pressure–force relation deviates only 0.0008% from the incompressible case.

The analytical calculated temperature error which is caused by the change in effective area equals for a steel boss and a steel membrane and a temperature increase of 30°C only 0.07%. This error can be compensated for by measuring the temperature.

By making the ratio r_1/r_2 close to one, the temperature error due to the difference in thermal expansion coefficients of the fluid and bucket is minimized. The error can also be minimized by matching these coefficients or by reducing the height d of the fluid. For the realized load cell, the analytical calculated error is 0.07%.

Analytical, numerical and experimental calculated pressure–force relations are in very close agreement with each other so that the analytical expressions can be very well used for designing purposes.

In order to eliminate the temperature dependence, unloading and loading the load cell was performed in 120 s. The experiments show a repeatability error of less than 0.025% which indicates that the desired accuracy of 0.03% is feasible. This repeatability was obtained by using a pressure sensor with a repeatability error within $\pm 0.15\%$. Measurements with a very accurate pressure sensor have to be performed to find out how much creep and hysteresis exactly are.

Acknowledgements

This research is supported by the Dutch Technology Foundation (STW).

References

[1] H. Kazerooni, M.S. Evans, J. Jones, Hydrostatic force sensor for robotic applications, Journal of Dynamic Systems, Measurement and Control 119 (1) (1997) 115–119.
[2] S.P. Timoshenko, S.W. Woinowsky-Krieger, Theory of Plates and Shells, McGraw-Hill International Editions, Singapore, 1959.
[3] R.W. Fox, A.T. McDonald, Introduction to Fluid Mechanics, 3rd edn., Wiley, Singapore, 1985.
[4] R.T. Fenner, Engineering Elasticity (Application of Numerical and Analytical Techniques), Wiley, New York, 1986.
[5] J.M. Gere, S.P. Timoshenko, Mechanics of Materials, Chappman and Hall, London, 1991.

Robert Zwijze was born in Almelo, The Netherlands, on January 10, 1973. He received his MSc degree in Mechanical Engineering from the University of Twente, Enschede, The Netherlands, in 1996 on the subject of modeling of large deformation behavior of aluminum. He is currently carrying out his PhD research at the department of electrical engineering at the same university on the subject of a silicon load cell. R. Zwijze enjoys playing soccer and politics.

Remco J. Wiegerink was born in Enschede, The Netherlands, on September 17, 1964. He received his MSc degree in Electrical Engineering from the University of Twente, Enschede, The Netherlands, in 1988 on the subject of a fully integrated ultra low frequency low-pass filter for offset cancelling in integrated audio amplifiers. In 1992, he received his PhD degree in Electrical Engineering at the same university on the subject of MOS translinear circuits. Between 1992 and 1995, he was with the Applied Physics department of the University of Twente, where he was engaged in the design of a superconductive flash analog-to-digital converter. He is now with the Micromechanical Transducers group at the MESA Research Institute at the University of Twente, where he is working on the design of a quasi-monolithic silicon load cell.

Gijs J.M. Krijnen was born 1961, in Laren, the Netherlands. He received his MSc degree in Electrical Engineering from the University of Twente following a study on magnetic recording carried out at the Philips Research Laboratories, Eindhoven, The Netherlands. From 1987 to 1992, he carried out his PhD research in the Lightwave Device Group of the MESA Research Institute at the University of Twente. In his PhD work, he investigated nonlinear integrated optics devices. In 1992, he became a fellow of the Royal Netherlands Academy of Arts and Sciences and studied second- and third-order nonlinear integrated optics devices. In 1993, he was the recipient of the Veder price of the Dutch Electronics and Radio Engineering Society (NERG). From 1993 to 1994, he was a visiting post-doc at the Center for Research and Education in Optics and Lasers in Orlando, Florida. 1995–1997 he worked as a postdoc on linear integrated optic devices at the University of Twente and the Delft University of Technology. In 1998, he started in the Micromechanics group of the MESA research institute. His current interests include (modeling of) MEMS, MOEMS, microfluidics, microsensor and microactuator devices.

Theo Lammerink was born in Tubbergen, the Netherlands, October 1956. He received his MSc degree in Electrical Engineering and his PhD from the University of Twente, in 1982 and 1989, respectively. His PhD research was focused on the optical excitation and read-out of micromechanical resonator sensors. He is member of the Micromechanical Transducers group of the MESA research institute. His research interests are on microliquid handling systems and integrated electromechanical microsystems.

Miko Elwenspoek (born December 9, 1948 in Eutin, Germany) studied physics at the Free University of Berlin (West). His thesis (MSc) dealt with Raleigh scattering from liquid glycerol using light coming from a Mössbauer source. From 1977–1979, he worked with Prof. Helfrich on lipid double layers. He conducted experiments on osmotic shrinkage of giant lipid vesicles, and while preparing light scattering experiments from those giant vesicles worked out the theory of light scattering from large aspheric particles and spherical bubbles. In 1979, he started his PhD work with Prof. Quitmann. This work dealt with relaxation measurements on liquid metals and alloys, in particular, alkali metal alloys. The experimental technique used in these experiments is related to nuclear magnetic resonance, but the alignment of the nuclei is done by a nuclear reaction using high energetic alpha radiation. This work resulted in a thesis (Freie Universität Berlin, 1983). In 1983, he moved to Nijmegen, The Netherlands, to study crystal growth in the group of Prof. Bennema of the University of Nijmegen. The emphasis lay on growth of organic crystals (in particular naphthalene) from melt and solution. In 1987, he went to the University of Twente, to take charge of the micromechanics group that was part of the Sensors and Actuators lab, now MESA Research Institute. Since then, his research focused on Microelectromechanical Systems. In the first years, the work was concentrated to coaching design and modeling of micropumps and resonant sensors by PhD students, but since the beginning of the ‘90s, more and more attendance was given to electrostatic microactuators, including electrostatic motors, and thermal and electromechanical actuators with the aim of building microrobots. Further, research in technology became more important, with emphasis on physical chemistry of wet chemical anisotropic etching, materials science of thin films (such as ZnO, TiNi, PZT and fluorocarbon), reactive ion etching of silicon, polymers and metals, wafer bonding and chemical–mechanical polishing. In 1996, he became full professor in transducer technology at the Faculty of Electrical engineering, University of Twente. M. Elwenspoek enjoys classical music, painting and drawing, and hiking.